Proc. Natl. Acad. Sci. USA
Vol. 78, No. 11, pp. 6863–6867, November 1981
Biophysics

Cholesteryl myristate conformation in liquid crystalline mesophases determined by neutron scattering

(cholesteryl ester/liquid crystal/atherosclerosis/low density lipoprotein/diffraction methods)

CHRISTIAN BURKS AND DONALD M. ENGELMAN*

Department of Molecular Biophysics and Biochemistry, Yale University, New Haven, Connecticut 06511

Communicated by Julian M. Sturtevant, June 15, 1981

ABSTRACT **The possible involvement of cholesteryl ester states in the development and persistence of atherosclerosis and the transport and storage of cholesteryl esters has led to questions concerning the organization and conformation of cholesteryl ester molecules in both pure phases and membranes. The experiments we report here were designed to measure the distance between the center of mass of the fatty acyl terminal methyl group and the center of mass of the three-carbon branched terminus of the cholesterol moiety at the opposite end of the molecule. The distance obtained is thus a gauge of cholesteryl ester conformation through the conformational range from a completely extended conformation to a U-shaped conformation. Neutron scattering experiments on partially deuterated samples of pure cholesteryl myristate in the crystalline, smectic, cholesteric, and isotropic phases indicate that the molecule is extended in each of these states. A discussion of specific molecular models consistent with these results and extension of these conclusions to other cholesteryl esters is included.**

Fatty acyl cholesteryl esters are characteristic of cholesterol storage and transport phenomena in mammals, including, in particular, humans. They are components of several serum lipoproteins (1–3); they appear in droplets just prior to nerve myelination in early development (4–6); they are present in milk and other extracellular fluids (7); they are also found in both the adrenal cortex (8) and ovaries (9); and they have been found associated with cellular membranes (10).

Cholesteryl ester deposits are also characteristic of several metabolic abnormalities, including degenerative neural diseases (most involving demyelination) (5, 11–14), disorders of the serum lipoprotein carrier system (3), and other conditions as well (15–17).

By far the most attention has been paid to the appearance of and role played by cholesteryl esters in atherosclerosis. The early stages of atherosclerosis are marked by the appearance of fatty streaks on the arterial wall. These contain high concentrations of lipid droplets, the main class of which is a group of long-chain fatty acyl cholesteryl esters (18–20).

Cholesteryl ester molecules are extremely hydrophobic and thus relatively insoluble in water and even, for the most part, in phospholipid (21). They therefore tend to form clusters, or "droplets," in an aqueous environment such as that of a cell's cytoplasm. Pure cholesteryl ester is liquid crystalline in characteristic temperature regions; that is, it passes through mesophases showing degrees of molecular order intermediate to the crystalline and isotropic phases upon heating or cooling (see Fig. 1). This behavior has been observed with cholesteryl ester droplets in isolated human atherosclerotic fatty streak tissue and in emulsions reflecting the lipid composition of droplets isolated from fatty streaks (23). It has also been observed that

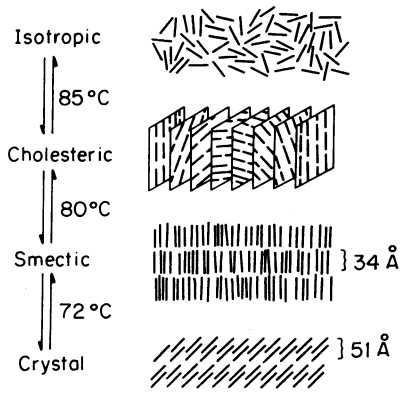

FIG. 1. Molecular organization of cholesteryl myristate as a function of temperature. The long axis of the molecule is depicted as a line segment. There is no long-term ordering in the isotropic phase; in the cholesteric phase the molecules line up end-to-end and in a given plane the lines are parallel, but the ends of the molecules are not in alignment (translation from plane to plane shifts the directions of the lines incrementally). The molecules in the smectic phase are packed into 34- to 35-Å-thick lamella forming a one-dimensional lattice. The details of the crystal structure are given by Craven and DeTitta (22).

at body temperature droplets can be found variously in the smectic, cholesteric, or isotropic phases (24).

These observations have led to the conjecture that differences in molecular conformation and intermolecular ordering in the several mesophases of cholesteryl ester droplets may affect cholesteryl ester interactions with enzymes and transport proteins at the droplet surface (23, 25, 26). It is thus of interest to determine what structural differences there are in the different phases of this lipid species.

The crystal structures of several cholesteryl esters have been solved and, to date, have shown an extended conformation in the crystalline state (27). In addition, cholesteryl esters have been studied with monolayer methods (28), x-ray scattering (29, 30), and magnetic resonance methods (31–40) in both the pure liquid crystalline and isotropic states and mixed with other lipids. However, none of these methods allows a direct determination of cholesteryl ester conformation in the noncrystalline states. Statements about conformation based on these approaches either involve extrapolation from the crystalline phase or rely heavily on assumptions about the cholesteryl ester structural motif.

The experiments reported here provide direct measurements of the distance between the two ends of cholesteryl myristate and, therefore, determine whether the molecule is extended or U-shaped (see Fig. 2) in its liquid crystalline and isotropic phases. The experimental strategy is analogous to that exploited in measuring subunit–subunit distances in the ribo-

The publication costs of this article were defrayed in part by page charge payment. This article must therefore be hereby marked "*advertisement*" in accordance with 18 U. S. C. §1734 solely to indicate this fact.

*To whom reprint requests should be addressed.

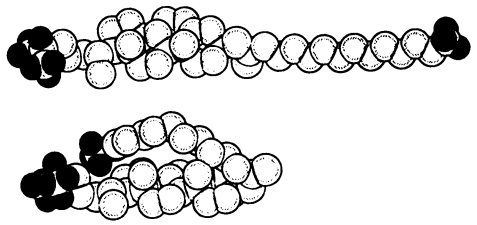

FIG. 2. Two possible conformations for cholesteryl myristate. The white spheres are the carbon and oxygen atoms; the shaded spheres are the hydrogen atoms chosen for substitution with deuterium (some of the ten atoms are partially or wholly occluded by other atoms in the orientations shown above). The centers of mass of the two deuterium substitution regions are 33.4 Å apart in the extended conformation and 7.2 Å apart in the U-shaped conformation. These conformations were generated by sequential bond rotation of an atomic coordinate system based on a modification of the coordinates given by Craven and DeTitta (22). Hydrogen atoms other than those shaded are not shown and were not taken into consideration in generating these conformations.

some (41); in this instance the strategy has been applied to intramolecular distances.

THEORY

On the basis of the work of Debye (42) and Zernicke and Prins (43), one can demonstrate that the scattering, $I(s)$, by a molecule in dilute solution is given by:

$$I(s) \propto \sum_i \sum_j f_i f_j \left[\frac{\sin(2\pi r_{ij}s)}{2\pi r_{ij}s}\right], \quad [1]$$

in which f_i and f_j are the atomic form factors of atoms i and j and r_{ij} is the distance between them. Both summations run over all atoms in a single molecule. The parameter s is related to the scattering angle at which $I(s)$ is measured, 2θ, by the equation $s = 2(\sin\theta)/\lambda$.

If we define a function, $p(r)$, such that:

$$p(r) = \sum_i \sum_j f_i f_j / f_{av}^2 \quad (r_{ij} = r), \quad [2]$$

in which $f_{av} = \Sigma f_i/N$ and N is the number of atoms in the molecule, then Eq. 1 may be recast (43, 44), ignoring proportionality constants and considering $p(r)$ as a continuous function, as:

$$I(s) = f_{av}^2 \int_0^\infty [p(r)\sin(2\pi rs)/2\pi rs]dr. \quad [3]$$

$p(r)$ is a "length distribution" function representing the distribution of interatomic vector lengths in the molecule. From Eq. 3 it can be seen that $p(r)$ is a spherical Fourier transform-mate of $I(s)$:

$$p(r) = (8\pi r/f_{av}^2) \int_0^\infty sI(s)\sin(2\pi rs)ds. \quad [4]$$

Thus, an experiment generating an $I(s)$ curve necessarily generates a $p(r)$ curve.

Consider the specific case of a molecule with two sites where deuterium atoms may be substituted for hydrogen atoms. Four distinct samples are possible: all-hydrogen (A), deuteration in both substitution sites (B), and the two samples with deuterium substitution at one site only (C and D). If the sum of the scattering intensity curves generated by C and D is subtracted from the sum of those of A and B, Eq. 1 reduces to (ignoring constants):

$$I_x(s) = 2(b_D - b_H) \sum_i \sum_j \left[\frac{\sin(2\pi r_{ij}s)}{2\pi r_{ij}s}\right]. \quad [5]$$

The subscripts i and j now respectively represent the atoms in the two separate substitution sites, and atomic form factors (f) have been exchanged for the scattering length (b) corresponding to neutron diffraction. If $I_x(s)$ is Fourier transformed to obtain its corresponding $p(r)$, the $p(r)$ function represents only the vectors between atoms in separate substitution sites.

Furthermore, one can obtain the distance, Δ_{ij}, between the centers of mass of the two substitution sites by the following relationship (41):

$$\Delta_{ij} = \int_0^\infty r^2 p(r)dr - R_1^2 - R_2^2, \quad [6]$$

in which R_1 and R_2 are the radii of gyration of the deuterium distributions of the two substitution sites and the integral represents the second moment of the normalized $p(r)$ curve.

If an equimolar mixture of A and B and an equimolar mixture of C and D are used as the two scattering samples (with scattering from the latter subtracted from the former), all intermolecular vectors will cancel out in $I_x(s)$. This allows preparation of quite concentrated solutions that generate data within the confines of the theoretical framework outlined above (45, 46).

MATERIALS AND METHODS

All-hydrogen cholesteryl myristate was acquired from Nu Check Prep (Elysian, MN) at >99% purity and was used without further purification. Three deuterated cholesteryl myristate samples were custom synthesized at >99% purity by Applied Science Laboratories (State College, PA): one sample with three deuterium atoms on the methyl carbon of the myristate chain, one sample with seven deuterium atoms on the branched terminus of the cholesteryl alkyl chain, and a third sample with deuterium in both of these sites. These samples were checked for purity by thin-layer chromatography and found to contain only trace impurities.

Quartz sample cells were custom manufactured by Precision Cells (Hicksville, NY). These were designed to facilitate sample loading through an overhead port and to allow sample expansion during temperature variation. An aluminum block was designed to hold four samples cells with a channel to allow temperature control by a circulating water bath.

Samples A and B were combined in equimolar quantities in a sample cell (I). The cell was heated to 100°C to eliminate air bubbles and possible water contamination and to promote mixing, and then centrifuged briefly. The heating and centrifuging cycle was repeated several times. A cell (II) containing equimolar amounts of samples C and D was prepared similarly, as was a cell (III) containing only sample A. A fourth cell (IV) was used for empty cell measurements.

The neutron scattering was carried out at the High Flux Beam Reactor at Brookhaven National Laboratory, using 2.33-Å neutrons. The experimental apparatus and data collection were as described (47, 48) in articles reporting distance measurements in the ribosome, with two exceptions: first, we used the linear sample changer described above, and second, because our samples consist of pure cholesteryl myristate and not a solution, our interference ripple is generated by using the simplified scheme:

$$I_x(s) = I_I(s) - (F_I/F_{II})\, I_{II}(s), \quad [7]$$

in which $I_I(s)$ is the scattering profile of the sample including the double-site deuterated cholesteryl myristate and $I_{II}(s)$ is that of the sample containing the single-site deuterated cholesteryl

myristates; F_I and F_{II} are the neutron transmissions through the corresponding samples.

Data processing was carried out using Glatter's (49) indirect transform algorithm as described (50) so as to generate, first, $p(r)$, second, a smooth fit to $I_x(s)$, and third, the second moment of $p(r)$ used in determining the end-to-end distance, Δ_{ij}, of the molecule together with appropriate error estimates.

RESULTS

Data determining interference scattering profiles were collected at four temperatures: 60.0, 77.0, 83.0, and 90.0°C, generating the crystalline, smectic, cholesteric, and isotropic phases, respectively, and providing a clear margin between the experimental temperature and the relevent transition temperatures (51). Observations of the deuterated and all-hydrogen cholesteryl myristate, using both a cross-polarized light microscope fitted with a temperature stage and the naked eye, demonstrated the usual phase transition temperatures (51), both before and after the experiments were run.

A preliminary run covering a broad region ($s = 0.005$ Å^{-1} to 0.085 Å^{-1}) of reciprocal space revealed that the data of interest to us were occurring in the $s < 0.04$ Å^{-1} region. The data we present here were therefore collected in the $s = 0.004$ Å^{-1} to $s = 0.037$ Å^{-1} region.

In the case of the smectic and isotropic phases, data were collected for 9 hr for each of the two samples contributing to the interference scattering profile (see Eq. 7). For the crystalline and cholesteric phases, data were collected for 4 hr for each of the two samples. The resulting interference scattering profiles are shown in Fig. 3, along with smooth fits generated by back-transformation of the corresponding length distribution profiles. The four profiles resemble each other and show no unusual features above noise. The data corresponding to Bragg reflections, at 1/51 Å^{-1} for the crystal phase and at 1/34 Å^{-1} for the smectic and cholesteric phases, were not due to the specific deuteration features of our samples, and were therefore omitted for data processing.

The length distribution profiles generated from the interference profiles in Fig. 3 are presented in Fig. 4. All four experiments have a relatively simple length distribution consisting of a single peak with a maximum in the 28- to 35-Å region; detail in the lower distance region (ranging from 0–15 Å to 0–25 Å) is within the calculated error envelopes for the length distributions and therefore unlikely to be significant. The width of

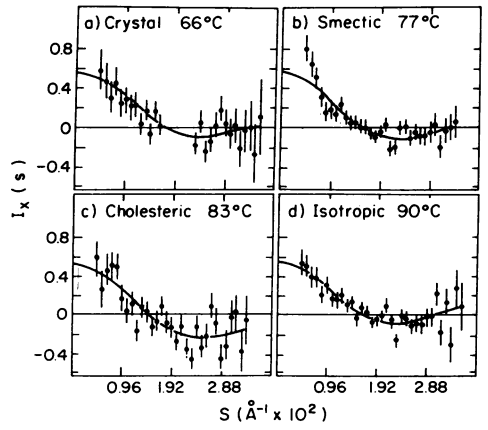

FIG. 3. Interference scattering profiles for cholesteryl myristate at 66.0°C (*a*), 77.0°C (*b*), 83.0°C (*c*), and 90.0°C (*d*). ●, Experimental profile; ——, smooth fit to data generated from corresponding length distribution profile in Fig. 4. The vertical bars are two standard errors (based on counting statistics only) in height.

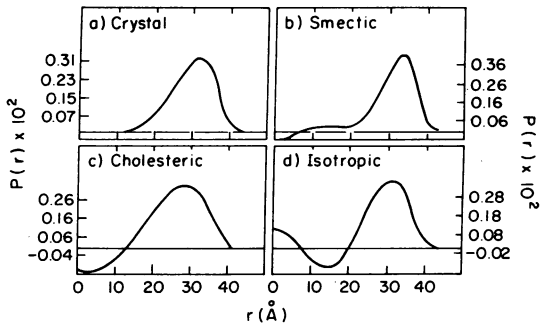

FIG. 4. Length distribution profile for cholesteryl myristate corresponding to the interference profiles for the four experimental temperatures: 66.0°C (*a*), 77.0°C (*b*), 83.0°C (*c*), and 90°C (*d*). These profiles were generated by using Glatter's indirect transform algorithm (49). The small excursions from the zero baseline in the short distance region (<20 Å) are within the predicted error envelopes for these profiles and are therefore uninterpretable.

the $p(r)$ curve is dependent on several factors: the spatial distribution of the deuterium atoms in the substitution sites, the resolving power of the indirect transform algorithm used to generate $p(r)$, and the distribution of conformations in the sample at a given moment in time.

The desired center-to-center distance (Δ_{ij}) is related to the second moment, $M_{ij} = \int_0^\infty r^2 p(r) dr$, of the normalized length distribution profile (see Eq. 6 in *Theory*). Calculation of Δ_{ij} requires, in addition to M_{ij}, values for the radii of gyration of the two substitution regions. These values can be calculated directly by modeling the three-deuterium and the seven-deuterium substitution regions with conventional bond lengths and bond angles for carbon–carbon and carbon–hydrogen bonds. The three-deuterium site gives $R_1^2 = 1.06$ Å^2 and the seven-deuterium site gives $R_2^2 = 3.37$ Å^2.

The center-to-center distances calculated for the two deuterium substitution regions at the ends of cholesteryl myristate are listed for each experimental temperature in Table 1. In the case of neutron scattering, the center of mass for each region is defined by the array of substitutable atomic nuclei locii.

The distances presented in Table 1 indicated that cholesteryl myristate is extended at each temperature of measurement.

DISCUSSION

Though several studies of noncrystalline phases have found data consistent with an extended conformation of various saturated and unsaturated long-chain fatty acyl cholesteryl esters, other molecular conformations would also be consistent with these data. Wendorff and Price (29) and McMillan (30) made small-angle x-ray diffraction measurements on the different phases of cholesteryl myristate and attributed the characteristic smec-

Table 1. Center-to-center distances, Δ_{ij}, for the two deuterium substitution regions at the ends of cholesteryl myristate

Phase	Δ_{ij}, Å
Crystal	30.3 ± 3.0
Smectic	31.8 ± 2.5
Cholesteric	28.4 ± 2.4
Isotropic	30.8 ± 2.5

Values for R_1^2 and R_2^2 used for the calculation were 1.06 Å^2 and 3.37 Å^2 (see Eq. 6 in *Theory*), assuming equal point masses at the substituted atomic nuclei loci. The second moments, M_{ij}, and their associated errors, σ_M, were calculated, after normalization, from the length distribution profiles, $p(r)$, in Fig. 3.

tic repeat diffraction peak at 33 Å to the long molecular axis. This coincides approximately with the modeled length, 37 Å, of extended cholesteryl myristate. However, other combinations of conformation (such as U-shaped) and packing motif would also be consistent with these data. Craven and DeTitta (22) with cholesteryl myristate and Atkinson *et al.* (52) with low-density lipoprotein also assumed an extended cholesteryl ester conformation in explaining the results of x-ray diffraction studies.

The end-to-end measurements reported here (see Table 1) provide a direct assessment of the conformation of cholesteryl myristate in the crystal, smectic, cholesteric, and isotropic phases. The Δ_{ij} value for the crystal, 30.3 ± 3.0 Å, agrees within error with a value, 33.4 Å, calculated with Craven and DeTitta's (22) atomic coordinates for crystalline cholesteryl myristate. The discrepancy, if significant, could be due to our crystal data being collected at 66.0°C whereas Craven and DeTitta's was collected at 25.0°C. This agreement provides independent verification of the validity of our approach. The values for the smectic (31.8 ± 2.5 Å), cholesteric (28.4 ± 2.4 Å), and isotropic (30.8 ± 2.5 Å) phases indicate that the molecule is extended in all phases. The value for the cholesteric phase is slightly lower than the others, but the difference is not statistically significant.

It should be noted that our results do not distinguish between mesophase packing models that have an extended molecular conformation in common. Both the model of Wendorff and Price (29) involving cholesterol–fatty acid antiparallel packing and that of Craven and DeTitta (22) involving cholesterol–cholesterol and fatty acid–fatty acid antiparallel packing are consistent with our findings.

It is of interest to consider whether these results are likely to hold for other long-chain cholesteryl esters, such as the biologically prevalent cholesteryl linoleate. Because these acyl chains are unsaturated, and may, therefore, contain kinks [see, however, Craven and Guerina's (53) crystallographic study of cholesteryl oleate], they may be less likely to be linearly extended. However, even if packing constraints allow the expected kink in these chains, the conformation of the molecule would still not be U-shaped in the sense of the ester bond being opposed to the two molecular termini. Further experiments similar to that reported here would provide direct measurements of the end-to-end distance of other cholesteryl ester molecules.

There is no reason to predict a change in conformation of a given long-chain cholesteryl ester between the pure bulk phase used in these experiments and the emulsions found in biological systems. There is a close correlation in structural and thermal mesophase behavior of cholesteryl ester between pure preparations, prepared emulsions, and emulsions of biological origin. This has been demonstrated in both the case of low density lipoprotein (54) and that of fatty streak lesion droplets (refs. 23 and 55 and unpublished results).

The extended conformation of cholesteryl esters may have an effect on cholesteryl ester transport and metabolism in the cell. Any interaction between a cytoplasmic enzyme and cholesteryl ester will take place at or near the interface between the cytoplasm's aqueous environment and the cholesteryl ester droplet's hydrophobic environment. This interface, in the case of cholesteryl ester droplets from atherosclerotic arteries, is thought to involve a monolayer of phospholipid (see Fig. 5), which provides an amphiphilic buffer between the cytoplasm and the droplet's interior. Whether or not an enzyme binds to the droplet surface, the state of the cholesteryl ester in the droplet could affect the formation rate of enzyme–cholesteryl ester complexes. For instance, in the smectic mesophase, the extended, radial disposition of the molecules places the ester

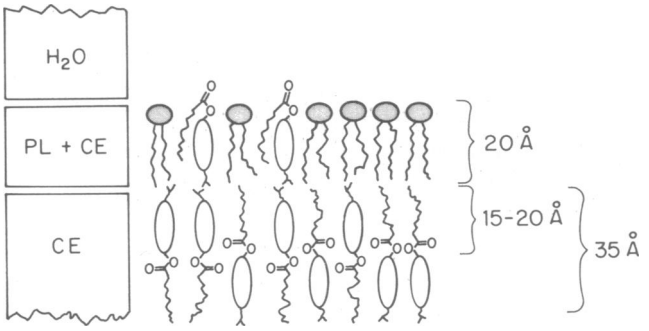

FIG. 5. Model for the surface region of the cholesteryl ester droplet in the smectic state. This surface consists of a monolayer of phospholipid molecules (PL) with a small amount of cholesteryl ester (CE) mixed in, depicted here in a U-shaped conformation. Several studies (21, 40) have suggested this conformation for cholesteryl ester in phospholipid bilayers. The cholesteryl ester molecules beneath the phospholipid monolayer are extended and arranged in radially repeating smectic lamella.

bonds themselves further from the interface than they would be in the isotropic phase, in which nonradial orientations may exist. Furthermore, the diffusion of cholesteryl ester to the surface of the droplet would be slower in the more ordered smectic and cholesteric phases than in the isotropic phase due to increased viscosities (56); diffusion would also be affected by the conformational change that would be necessary in moving a molecule from the droplet core to the droplet surface in such a way as to bring the ester bond to the water–droplet interface (see Fig. 5). The conformational constraint forces the enzyme–cholesteryl ester interaction to be restricted to the droplet surface and the viscosity constraint makes an enzyme–cholesteryl ester interaction much less likely in the smectic and cholesteric phases.

Experiments in our laboratory have shown that cholesterol esterase (EC 3.1.1.13) is considerably depressed when acting on cholesteryl ester–egg lecithin droplets in the cholesteric and smectic states as compared to acting on droplets in the isotropic state (unpublished results).

Our experimental result that cholesteryl myristate is extended in all states and its implications for metabolic control of cholesteryl ester may apply to several structures containing cholesteryl ester other than the fatty streak droplets discussed herein. An example is the low density lipoprotein, which is thought to consist in part of a cholesteryl ester core, the state of which may affect metabolism of these particles (57).

We are grateful for technical support from G. Johnson and E. Caruso and the helpful expertise of V. Ramakrishnan and I. Sillers. The experiments at the High Flux Beam Reactor at Brookhaven National Laboratory were carried out under the auspices of the U.S. Department of Energy. This work was supported by the National Institutes of Health (USPHS-HL-14111) and the National Science Foundation (PCM-78-10361). C.B. was supported in part by National Institutes of Health Training Grant USPHS-2-GM07223.

1. Levy, R. I., Bilheimer, D. W. & Eisenberg, S. (1971) *Biochem. Soc. Symp.* **33**, 3–17.
2. Skipski, V. P. (1972) in *Blood Lipids and Lipoproteins: Quantitation, Composition and Metabolism*, ed. Nelson, G. (Wiley–Interscience, New York), pp. 471–583.
3. Skipski, V. P., Barclay, M., Barclay, R. K., Fetzer, V. A., Good, J. J. & Archibald, F. M. (1967) *Biochem. J.* **104**, 340–352.
4. Paoletti, R., Grossi-Paoletti, E. & Fumagalli, R. (1969) in *Handbook of Neurochemistry*, ed. Lajtha, A. (Plenum, New York), Vol. 1, pp. 195–222.
5. Davison, A. N. (1965) *Adv. Lipid Res.* **3**, 171–196.

6. Davison, A. N. (1970) in *Handbook of Neurochemistry*, ed. Lajtha, A. (Plenum, New York), Vol. 3, pp. 547–560.
7. Sabine, J. R. (1977) *Cholesterol* (Dekker, New York).
8. Riley, C. (1963) *Biochem. J.* **87**, 500–507.
9. Stewart, G. T. (1967) *Adv. Chem.* **63**, 141–156.
10. Zambrano, R., Fleischer, S. & Fleischer, B. (1975) *Biochim. Biophys. Acta* **380**, 357–369.
11. Ramsey, R. B. & Nicholas, H. J. (1972) *Adv. Lipid Res.* **10**, 143–232.
12. Ramsey, R. B. & Davison, A. N. (1974) *J. Lipid Res.* **15**, 249–255.
13. Rouser, G. & Yamamoto, A. (1969) in *Handbook of Neurochemistry*, ed. Lajtha, A. (Plenum, New York), Vol. 1, pp. 121–169.
14. Guazi, G. C. & van Bogaert, L. (1969) in *The Structure and Function of the Nervous System*, ed. Bourne, G. H. (Academic, New York), Vol. 3, pp. 383–439.
15. Takeuchi, N. & Yamamura, Y. (1973) *Atherosclerosis* **17**, 211–224.
16. Sloan, H. R. & Fredrickson, D. S. (1972) in *The Metabolic Basis of Inherited Disease*, eds. Stanbury, J. B., Wyngaarden, J. B. & Fredrickson, D. S. (McGraw-Hill, New York), 3rd Ed., pp. 808–832.
17. Duke, J. R. & Woods, A. C. (1963) *Br. J. Ophthalmol.* **47**, 413–434.
18. Smith, E. S., Evans, P. H. & Bownham, M. D. (1967) *J. Atheroscler. Res.* **7**, 171–186.
19. Smith, E. S. (1965) *J. Atheroscler. Res.* **5**, 224–240.
20. Lang, P. D. & Insull, W. (1970) *J. Clin. Invest.* **49**, 1479–1488.
21. Janiak, M. J., Loomis, C. R., Shipley, G. G. & Small, D. M. (1974) *J. Mol. Biol.* **86**, 325–339.
22. Craven, B. M. & DeTitta, G. T. (1976) *J. Chem. Soc. Perkin Trans. 2*, 814–822.
23. Engelman, D. M. & Hillman, G. M. (1976) *J. Clin. Invest.* **58**, 997–1007.
24. Hillman, G. M. & Engelman, D. M. (1976) *J. Clin. Invest.* **58**, 1008–1018.
25. Hata, Y. & Insull, W. (1973) *Jpn. Circ. J.* **37**, 269–275.
26. Small, D. M. & Shipley, G. G. (1974) *Science* **185**, 222–229.
27. Sawzik, P. & Craven, B. M. (1980) in *Liquid Crystals*, ed. Chandrasekhar, S. (Heyden, Philadelphia), pp. 171–178.
28. Smaby, J. M. & Brockman, H. L. (1981) *Biochemistry* **20**, 718–723.
29. Wendorff, J. H. & Price, F. P. (1973) *Mol. Cryst. Liquid Cryst.* **24**, 129–144.
30. McMillan, W. L. (1972) *Phys. Rev. A.* **6**, 936–947.
31. Runyan, W. R. & Nolle, A. (1957) *J. Chem. Phys.* **27**, 1081–1087.
32. Dybowski, C. R. & Wade, C. G. (1971) *J. Chem. Phys.* **55**, 1576–1578.
33. Cutler, D. (1969) *Mol. Cryst. Liquid Cryst.* **8**, 85–92.
34. Matthews, R. M. C. & Wade, C. G. (1975) *J. Magn. Reson.* **19**, 166–172.
35. Sears, B., Deckelbaum, R. J., Janiak, M. J., Shipley, G. G. & Small, D. M. (1976) *Biochemistry* **15**, 4151–4157.
36. Hamilton, J. A., Oppenheimer, N. & Cordes, E. H. (1977) *J. Biol. Chem.* **252**, 8071–8080.
37. Valic, M. I., Gorrissen, H., Cushley, R. J. & Bloom, M. (1979) *Biochemistry* **18**, 854–859.
38. Gorrissen, H., Tulloch, A. P. & Cushley, R. J. (1980) *Biochemistry* **19**, 3422–3429.
39. Grover, A. K. & Cushley, R. J. (1979) *Atherosclerosis* **32**, 87–91.
40. Grover, A. K., Forrest, B. J., Buchinski, R. K. & Cushley, R. J. (1979) *Biochim. Biophys. Acta* **550**, 212–221.
41. Moore, P. B., Langer, J. A. & Engelman, D. M. (1978) *J. Appl. Crystallogr.* **11**, 479–482.
42. Debye, P. (1915) *Ann. Phys. (Leipzig)* **46**, 809–823.
43. Zernicke, F. & Prins, J. A. (1927) *Z. Phys.* **41**, 184–194.
44. Moore, P. B. (1981) in *Biophysical Methods*, Methods in Experimental Physics, eds. Ehrenstein, G. & Lecar, H. (Academic, New York), Vol. 20, in press.
45. Hoppe, W. (1972) *Isr. J. Chem.* **10**, 321–333.
46. Hoppe, W. (1973) *J. Mol. Biol.* **78**, 581–585.
47. Moore, P. B., Langer, J. A., Schoenborn, B. P. & Engelman, D. M. (1977) *J. Mol. Biol.* **112**, 199–234.
48. Engelman, D. M. (1979) *Methods Enzymol.* **59**, 656–669.
49. Glatter, O. (1977) *Acta Phys. Austr.* **47**, 83–102.
50. Schindler, D. G., Langer, J. A., Engelman, D. M. & Moore, P. B. (1979) *J. Mol. Biol.* **134**, 595–620.
51. Barrall, E. M., Porter, R. S. & Johnson, J. F. (1967) *Mol. Cryst.* **3**, 103–115.
52. Atkinson, D., Deckelbaum, R. J., Small, D. M. & Shipley, G. G. (1977) *Proc. Natl. Acad. Sci. USA* **74**, 1042–1046.
53. Craven, B. M. & Guerina, N. G. (1979) *Chem. Phys. Lipids* **24**, 91–98.
54. Deckelbaum, R. J., Shipley, G. G., Small, D. M., Lees, R. S. & George, P. K. (1975) *Science* **190**, 392–394.
55. Lundberg, B. (1975) *Chem. Phys. Lipids* **14**, 309–312.
56. Sakamoto, J., Porter, R. S. & Johnson, J. F. (1969) *Mol. Cryst. Liquid Cryst.* **8**, 443–455.
57. Deckelbaum, R. J., Shipley, G. G. & Small, D. M. (1977) *J. Biol. Chem.* **252**, 744–754.